THE JOURNAL OF PHYSICAL CHEMISTRY C

pubs.acs.org/JPCC Article

Pressure-Induced Selective Amorphization of $CsPbBr_3$ for the Purification of Cs_4PbBr_6

Lan Anh Thi Nguyen, Duong Nguyen Minh, Dongzhou Zhang, Lin Wang,* Jaeyong Kim,* and Youngjong Kang*

Cite This: J. Phys. Chem. C 2020, 124, 22291−22297 Read Online

ACCESS | Metrics & More | Article Recommendations | Supporting Information

ABSTRACT: Lead halide perovskites have been of great interest due to their promising optoelectronic applications. While solution-based synthetic methods have been well developed, they often form mixtures of perovskites having several different phases, which cannot be easily purified by conventional purification methods. Here we report a high-pressure purification method of 0D Cs_4PbBr_6 perovskite containing a trace of 3D $CsPbBr_3$. The synthesized 0D Cs_4PbBr_6 perovskites exhibit strong photoluminescence at λ_{peak} = ∼520 nm because of the trace amount of $CsPbBr_3$ embedded in the Cs_4PbBr_6. With the application of high pressure (20 GPa), the crystalline $CsPbBr_3$ phase turns amorphous, while the crystal structure of Cs_4PbBr_6 is retained without change. Almost 95% of the $CsPbBr_3$ phase can be removed by one cycle of compression (1 atm to 20 GPa, and to 1 atm). Due to the removal of $CsPbBr_3$, Cs_4PbBr_6 perovskites which originally show strong green fluorescence become nonfluorescent after one cycle of compression.

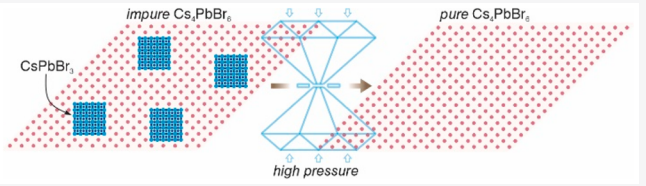

INTRODUCTION

Impurities affect the properties of materials. In particular, the optical and electrical properties of original materials are significantly altered by the trace amount of impurities. Since the localized electronic states (so-called trap states) in semiconducting materials are strongly associated with chemical impurities,[1,2] their properties such as absorption, emission, conductivity, and carrier mobility are dependent on impurities. Hence, purification techniques or controlled impurity levels in materials are in high demand for their application. For organic materials, various purification methods including distillation, sublimation, crystallization, and chromatography have been well developed. Alternatively, purification techniques for inorganic materials are relatively limited. Furthermore, it is very difficult to purify inorganic nanomaterials with different size, dimensionality, and phase, which are also crucial factors to affect their optical and electric properties.

In recent years, metal halide perovskites (MHPs) with the formula $A_\alpha BX_{2+\alpha}$, where A, B, and X are monovalent cations, divalent metals such as Pb^{2+}, and halogen anions such as Cl^-, Br^-, and I^-, respectively, have been of great interest due to their outstanding optical and electrical properties.[3−8] In this case, α can vary from 1 to 4. For the case of α = 1 (ABX_3), it forms a typical three-dimensional (3D) structure. Increasing α leads to the formation of lower dimensional structures and ultimately zero-dimensional (0D) perovskites (A_4BX_6) are formed when α is 4. More recently, low dimensional MHPs have begun to receive increasing attention because of their strong quantum confinement and high stability. For example, 0D Cs_4PbBr_6 perovskites have been investigated as a promising wide band gap material (E_{gap} > 3.0 eV),[9−11] with the intent of their application in UV detectors.[12,13] Originally, 0D Cs_4PbBr_6 perovskites attracted research interest because of their very high photoluminescence quantum yield (PLQY = 45%) in the solid state, which is almost 2 orders higher than that of 3D $CsPbBr_3$.[14−18] However, it turns out that pure 0D Cs_4PbBr_6 is nonfluorescent at room temperature due to the thermal quenching caused by exciton migration, and the frequently observed green emission (λ = ∼520 nm) in Cs_4PbBr_6 is more likely the result of emission by $CsPbBr_3$ embedded in bulk Cs_4PbBr_6.[19] In this case, the impurity, $CsPbBr_3$ embedded in Cs_4PbBr_6, is not easily removed using conventional purification methods such as solvent treatment, thermal treatment, and centrifugation.

In this work, we report an efficient purification method of 0D Cs_4PbBr_6 containing an impurity of 3D $CsPbBr_3$ by high-pressure compression. Our approach utilized the fact that 3D $CsPbBr_3$ crystals are sensitive to the change of pressure and generate distortions of the Pb−Br bonds at moderately low pressure, while 0D Cs_4PbBr_6 crystals are much more stable at high pressure conditions.[20,21] The selective amorphization of 3D $CsPbBr_3$ crystals was induced by applying high pressure. After decompression, the content of $CsPbBr_3$ decreased

Received: July 13, 2020
Revised: September 10, 2020
Published: September 14, 2020

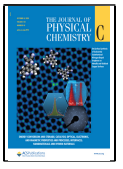

https://dx.doi.org/10.1021/acs.jpcc.0c06405
J. Phys. Chem. C 2020, 124, 22291−22297

significantly. The purity of Cs_4PbBr_6 bulk crystals was confirmed by photoluminescence (PL), UV−vis absorbance, XRD, and Raman measurements.

EXPERIMENTAL SECTION

Sample Preparation and High-Pressure Generation. All reagents including cesium bromide (CsBr, 99.9%, Sigma-Aldrich), lead bromide (PbBr2, 98%, Sigma-Aldrich), and dimethyl sulfoxide (DMSO, ≥99.5%, Daejung, Korea) were used as-received without further purification. Cs_4PbBr_6 crystals were synthesized by the antisolvent vapor-assisted crystallization (AVC) method.[22] Briefly, a crystallization vial containing 1 mL of precursor solution of 0.25 M lead bromide ($PbBr_2$) and 0.25 M cesium bromide (CsBr) in dimethyl sulfoxide (DMSO) was placed inside of a closed container with 4 mL of diethyl ether under room conditions. Due to the high vapor pressure of diethyl ether at room temperature, Cs_4PbBr_6 crystals formed by the gradual diffusion of diethyl ether into the vial. After 48 h, an interface between diethyl ether and DMSO was formed in the vial, resulting in the growth of small crystals. The crystals were collected and washed with ample amounts of IPA/DMSO (3:1) solvent and then dried in nitrogen atmosphere. High pressure experiments were carried out using a symmetric diamond anvil cell (DAC). A T301 stainless steel gasket with a thickness of 250 μm was used as the sample chamber. An approximately 5 μm ruby ball was inserted into the sample compartment for in situ pressure calibration. Silicone oil was used as the pressure transmitting medium. The compression was carried out an interval of about 30 min per step.

Optical Absorbance, PL, and Raman Measurements. Absorbance spectra were taken in the exciton absorption band region using a deuterium-halogen light source. PL spectra were collected using a Horiba LabRAM HR Evolution Raman spectrometer, equipped with a 473 nm laser. In situ high pressure Raman spectra were recorded using a silicon CCD detector. A Renishaw Via Raman system was used to collect the Raman signal from the sample in a DAC. A 633 nm radiation of a He−Ne laser with 17 mW output power was used to excite the sample.

XRD Measurements. High pressure XRD data were measured at 13BMC of the Advanced Photon Source at the Argonne National Laboratory. The Dioptas program was used to integrate and analyze the collected 2D images. The XRD patterns were refined using the crystallography data analysis program of the General Structure Analysis System (GSAS).

RESULTS AND DISCUSSION

Cs_4PbBr_6 bulk crystals were prepared by following the antisolvent vapor-assisted crystallization method.[22] Briefly, a crystallization vial containing 1 mL of precursor solution of 0.25 M lead bromide ($PbBr_2$) and 0.25 M cesium bromide (CsBr) in dimethyl sulfoxide (DMSO) was placed inside a closed container with 4 mL of diethyl ether at room conditions. Due to the high vapor pressure of diethyl ether at room temperature, Cs_4PbBr_6 crystals formed by the gradual diffusion of diethyl ether into the vial. After 48 h, an interface between diethyl ether and DMSO was formed in the vial, resulting in the growth of small crystals. The crystals were collected and washed with ample amount of IPA/DMSO (3:1) solvent then dried in nitrogen atmosphere.

As-prepared Cs_4PbBr_6 crystals exhibited a pale green color under visible light, and a bright green fluorescence under UV light, as shown in Figure 1a,b. To explore their optical

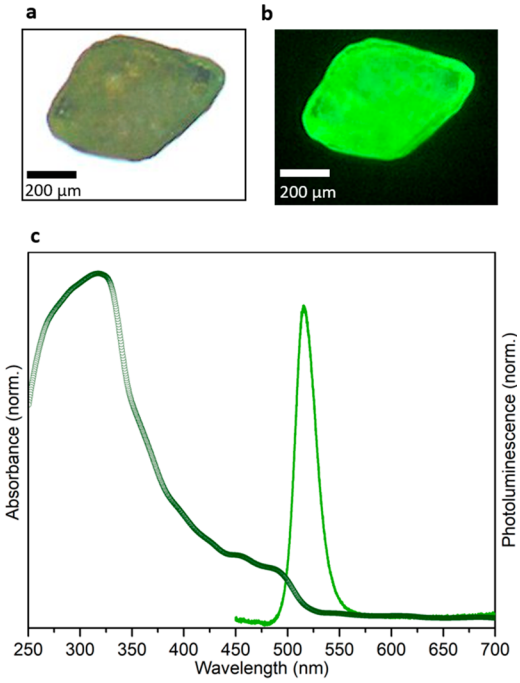

Figure 1. (a) Optical and (b) fluorescence micrographs of a Cs_4PbBr_6 crystal. (c) Absorption spectrum (dark green dots) and PL spectrum (light green line) of a bulk Cs_4PbBr_6 crystal.

properties, absorption and emission spectra were obtained. As shown in Figure 1c, a strong absorption peak around at 320 nm (3.87 eV) that corresponds to the absorption band of Cs_4PbBr_6 was observed.[15,23,24] In addition to the Cs_4PbBr_6 peak, another absorption edge at 528 nm (2.36 eV) was also detected. Additionally, the crystal exhibited a sharp PL peak at λ_{em} = 515 nm with a narrow bandwidth (fwhm = 22 nm) with exposure of UV light (λ_{ex} = 325 nm). It is notable that the PL emission was higher than the band gap obtained by absorption. We attributed that this is mainly because of the inaccurate estimation of absorption edge. The Tauc analysis used in our experiments is convenient, but the Tauc band gap tends to underestimate the electronic band gap due to the presence of excitonic transition.[25,26] Both the absorption edge at 528 nm and the PL at 515 nm correspond to the typical features of 3D $CsPbBr_3$ nanoparticles. These results suggest that the synthesized 0D Cs_4PbBr_6 crystals are not pure but rather a mixture with 3D $CsPbBr_3$. Due to the inhomogeneous distribution of 3D $CsPbBr_3$ in 0D Cs_4PbBr_6, some parts of the Cs_4PbBr_6 crystal look transparent and nonemissive under both visible and UV irradiation, and consistently there was no absorption and emission signal.

Crystal structure of the synthesized Cs_4PbBr_6 was characterized by analyzing synchrotron X-ray diffraction (XRD) data. The collected XRD data were compared with the calculated one to validate the purity of the synthesized Cs_4PbBr_6 crystal (Figure 2). It was confirmed that the structure of the sample was 0D Cs_4PbBr_6, a rhombohedral phase with space group $R\bar{3}c$ based on the refined XRD results at ambient condition. The unit cell dimensions are $a = b =$ 13.72 Å, c = 17.30 Å. The structure of Cs_4PbBr_6 crystal consists

https://dx.doi.org/10.1021/acs.jpcc.0c06405
J. Phys. Chem. C 2020, 124, 22291−22297

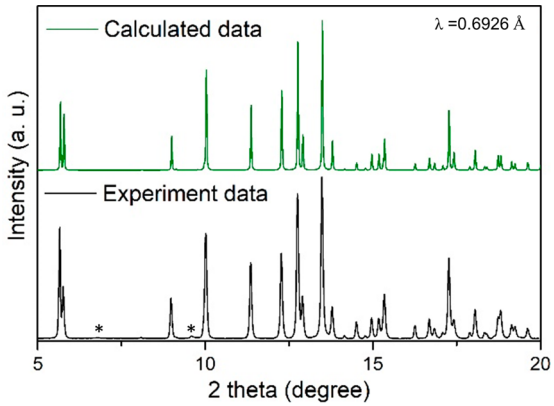

Figure 2. Powder XRD pattern of the synthesized Cs_4PbBr_6 crystal (black). The peaks marked with asterisk correspond to $CsPbBr_3$ phase. The calculated XRD pattern of Cs_4PbBr_6 (green) is well matched with the experimental one.

of isolated octahedral $PbBr_6^{-4}$ ions and interspersed Cs^+ cations (Figure S1 of the Supporting Information, SI). Along with the characteristic patterns of Cs_4PbBr_6, some other small peaks were also found in the XRD. Those peaks corresponded to the diffraction pattern of $CsPbBr_3$ with space group $Pm\bar{3}m$ and lattice constant a = 5.90 Å (Figure S2). Considered together with UV−vis and PL features, XRD analyses support that the synthesized Cs_4PbBr_6 crystals contain a small amount of $CsPbBr_3$ as an impurity, and the strong green fluorescent emission at λ_{em} = 515 nm originates from the impurity $CsPbBr_3$ embedded in Cs_4PbBr_6. In this case, $CsPbBr_3$ crystallites are expected to be uniformly embedded in the Cs_4PbBr_6 crystal due to endotaxial stabilization.[27−30]

Hence, $CsPbBr_3$ was not easily removed from Cs_4PbBr_6 using conventional solvent treatment. As mentioned earlier, although the synthesized Cs_4PbBr_6 crystals were washed with solvents, the characteristics of $CsPbBr_3$ (absorption edge at 528 nm and PL at 515 nm) kept appearing regardless of the solvent treatments. As an alternative purification method, we have utilized high-pressure compression. Figure 3a shows the representative in situ high-pressure optical micrographs of a Cs_4PbBr_6 crystal in a diamond anvil cell (DAC). Originally, the crystal was transparent with a pale yellow color. With compression, the yellow color gradually became weaker, and almost disappeared at 3.3 GPa. Above 3.3 GPa, the crystal again turned to a pale orange color, which became a deeper and deeper color as the pressure increased to 20.0 GPa. After releasing the pressure to 1 atm, the crystal looked completely colorless and transparent. The fluorescent photographs at the corresponding pressure were also observed. As shown in Figure 3b, the Cs_4PbBr_6 crystal exhibited strong green fluorescence at 1 atm due to the trace amount of $CsPbBr_3$ as previously discussed. With increasing pressure, the green fluorescent color gradually diminished and became almost nonfluorescent at 3.3 GPa. With further compression above 3.3 GPa, the sample started to show yellow fluorescence at 6.3 GPa, whose intensity increased until ∼12.0 GPa. However, the fluorescence became weaker again above 14.5 GPa, and then finally turned colorless above 20.0 GPa. After decompression to 1 atm, the sample was still almost nonfluorescent.

Selected steady-state pressure-dependent PL spectra are shown in Figure 4a. The PL spectrum at 1 atm showed a strong peak at 515 nm, which again was attributed to the PL of impurity $CsPbBr_3$ embedded in the Cs_4PbBr_6. The PL intensity was gradually decreased with increasing pressure, and eventually disappeared above 2.2 GPa. The disappearance

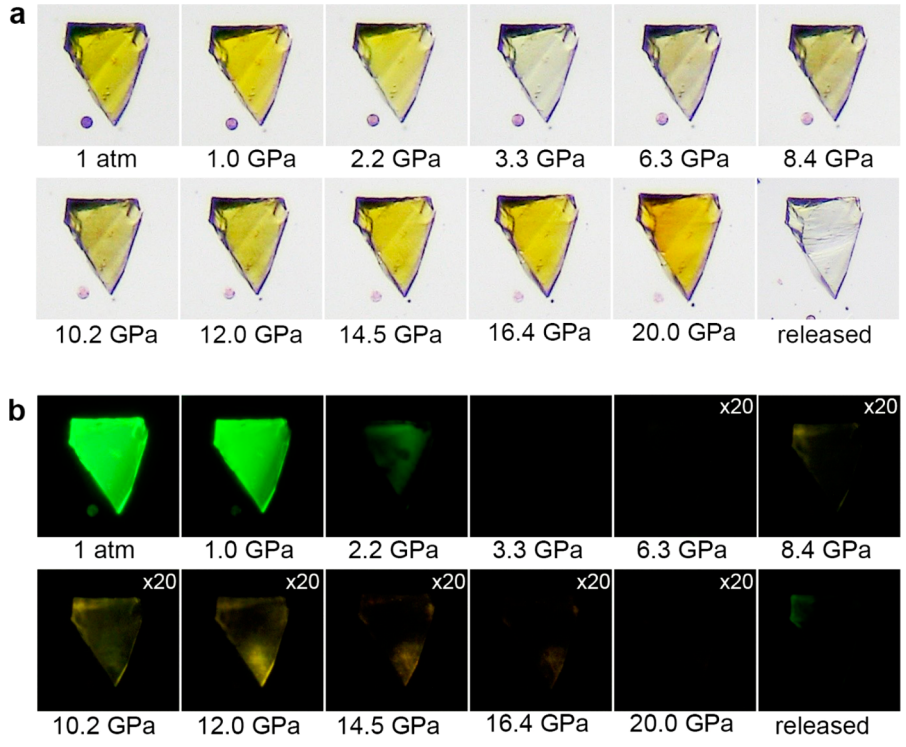

Figure 3. (a) In situ high-pressure optical micrographs in a DAC showing the piezochromism of a Cs_4PbBr_6 crystal. (b) Corresponding PL photographs under UV irradiation. Exposure times were increased by 20 times in the pressure range of 6.3−20.0 GPa.

https://dx.doi.org/10.1021/acs.jpcc.0c06405
J. Phys. Chem. C 2020, 124, 22291−22297

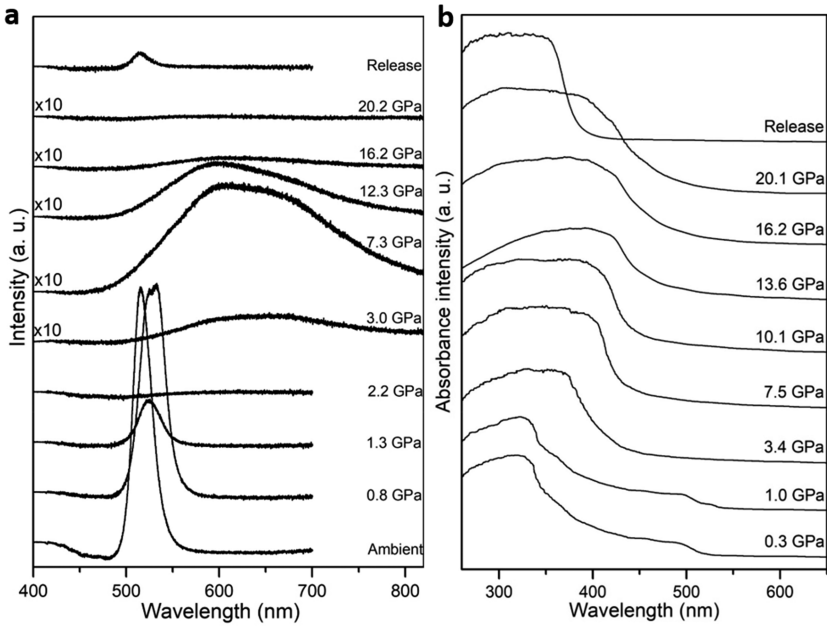

Figure 4. (a) PL spectra and (b) absorption spectra of Cs_4PbBr_6 crystal as a function of the compressive pressure.

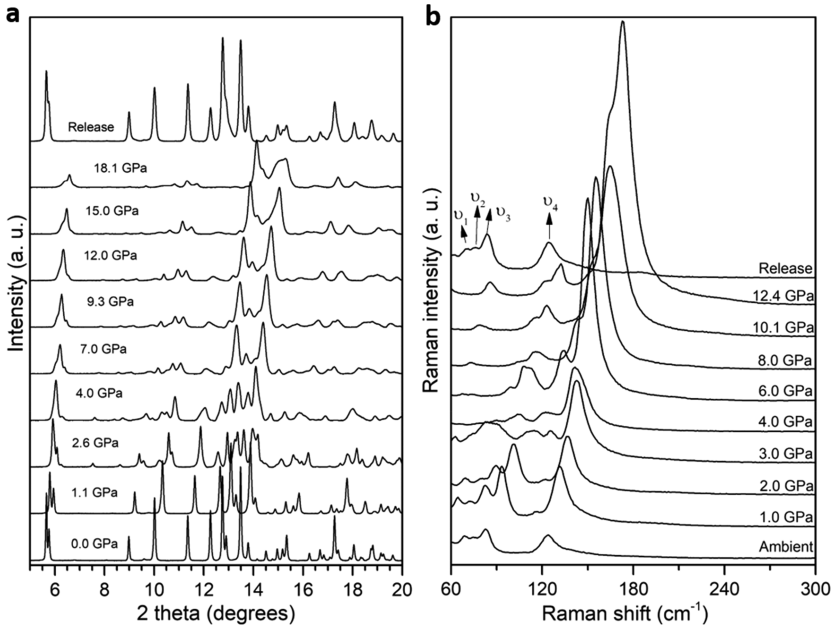

Figure 5. (a) Representative XRD patterns and (b) Raman spectra of Cs_4PbBr_6 crystals measured at different pressure levels.

of PL peak at 515 nm corresponds to the pressure-induced amorphization of $CsPbBr_3$.[20,21] The sample exhibited a very broad emission peak centered ~600 nm above 7.3 GPa, which is a characteristic feature of a Cs_4PbBr_6 crystal under high pressure.[31] The broad PL emission of Cs_4PbBr_6 appearing at high pressure was attributed to the charge carrier relaxation by the self-trapped exciton (STE) state (Figure S3).[31−33] Since its PL intensity was much weaker than that of PL peak 515 nm, the PL spectra above 3.0 GPa were presented by multiplying 10 times to clearly show the peak at ~600 nm (Figure 4a). The PL intensity increased as the pressure increased up to 12.3 GPa, and then decreased again when the pressure increased to 20.2 GPa. No emission was observed above 16.2 GPa. Such PL intensity changes are consistent with the PL responses of Cs_4PbBr_6 nanocrystals reported elsewhere.[31] After decompression to 1 atm, the PL peak recovered at 515 nm, but the intensity significantly reduced (less than 5% of the original PL intensity at 1 atm). The in situ high pressure absorption spectra of the crystals were also collected in Figure 4b. The band edge at 528 nm attributed to the absorption by $CsPbBr_3$ gradually disappeared as the pressure increased. The disappearance of the band edge corresponds to the disappearance of the green fluorescence of $CsPbBr_3$. These data strongly suggest that the impurity $CsPbBr_3$ was removed by pressure-induced amorphorization. When the pressure increased to 3.4 GPa, the absorption peak at 320 nm of Cs_4PbBr_6 became broadened and the edge was extended to the visible range. Ma et al. reported that this phenomenon was caused by the binding energy of self-trapped excitons upon the large distortion of $[PbBr_6]^{-4}$ octahedral motifs of the Cs_4PbBr_6

https://dx.doi.org/10.1021/acs.jpcc.0c06405
J. Phys. Chem. C 2020, 124, 22291−22297

crystal resulting from pressure.[31] After decompression, the absorption peak of the Cs_4PbBr_6 crystal recovered to a broad peak at 310 nm, but the band edge of $CsPbBr_3$ was not recuperated.

In situ XRD and Raman experiments more clearly conform the purification of Cs_4PbBr_6 crystal by compression. XRD patterns of Cs_4PbBr_6 were obtained as a function of pressure (Figure 5a). The diffraction peaks of $CsPbBr_3$ quickly decreased with increasing pressure, and then totally disappeared at 2.6 GPa. Meanwhile, the evolution of the XRD patterns demonstrates that a reversible phase transition of Cs_4PbBr_6 from a rhombohedral (space group $R\bar{3}c$) to a monoclinic (space group B2/b) structure began at 2.6 GPa (Figure S4). The phase transition is accompanied by the distortion of $[PbBr_6]^{-4}$ octahedra, which can lead to the increased binding energy of self-trapped excitonic state of the material. We carried out the high-pressure Raman experiments to track the impact of the Pb−Br network structure on the optical properties of the sample. The evolution of Raman spectra in the range of 60 to 300 cm^{-1} is shown in Figure 5b. There are four strong peaks at 69, 74, 82, and 123 cm^{-1}, corresponding to υ_1, υ_2, υ_3, and υ_4 vibrational modes, respectively, observed under ambient conditions. These modes were assigned for the vibrational modes of the $[PbBr_6]^{-4}$ octahedron and the motion of Cs^+.[16,34] With increasing pressure, all Raman peaks moved continuously to the higher frequency regime, indicating pressure-induced Pb−Br bond contraction. The profile of the spectra remained unchanged, but the intensity varied with the pressure. The υ_1, υ_2, and υ_3 modes became very weak and almost disappeared as the pressure increased higher than 2.0 GPa. The reduction in intensity of these modes is possibly because of the change of Pb−Br network structure caused by the pressure-induced $[PbBr_6]^{-4}$ octahedral distortion. Meanwhile, the relative intensity of the υ_4 mode was enhanced, especially over 4.0 GPa. The three modes υ_1, υ_2, and υ_3 redistribute those intensities at 2.0 GPa, which agrees well with the Rietveld refinement results, reflecting that the phase transition of Cs_4PbBr_6 crystals was caused by the change of the octahedral structure, followed by amorphization above 5.0 GPa. After decompression, both XRD patterns and Raman profiles of Cs_4PbBr_6 recovered their original state at ambient conditions, which suggests that the structure of Cs_4PbBr_6 crystal was reversible.

These all results strongly suggest that the high-pressure compression to 20 GPa leads to the selective amorphization of $CsPbBr_3$ without deteriorating the structure of Cs_4PbBr_6. The removal efficiency of $CsPbBr_3$ from Cs_4PbBr_6 crystal by single compression was remarkably high (>95%). When the compression pressure is lower than 20 GPa, the purification efficiency decreased. The purification efficiency was lowered to ~60% when the compression pressure was 17 GPa (Figure S5). Hence at least three compression cycles were demanded to achieve the similar purification efficiency at 20 GPa when the compression pressure was 17.0 GPa (Figure S6). Once $CsPbBr_3$ crystallites were amorphorized, they barely recrystallized under ambient conditions. As shown in Figure S7, Cs_4PbBr_6 crystal stayed nonfluorescent at least for 10 days after our high pressure purification.

CONCLUSIONS

In summary, a novel purification method of Cs_4PbBr_6 crystal was developed. High-pressure compression can be used to selectively remove $CsPbBr_3$ by pressure-induced amorphization without depreciating the Cs_4PbBr_6 crystal structure. After purification, the remaining amount of $CsPbBr_3$ embedded in Cs_4PbBr_6 was almost negligible, and the crystallinity of Cs_4PbBr_6 was intact. We anticipate that our purification method is suitable for obtaining highly crystalline Cs_4PbBr_6 crystals without $CsPbBr_3$ impurity and potentially applicable for other semiconducting materials.

ASSOCIATED CONTENT

Supporting Information

The Supporting Information is available free of charge at https://pubs.acs.org/doi/10.1021/acs.jpcc.0c06405.

Additional figures showing all XRD with Le-Bail refinement details, PL spectra, and fluorescent photographs at high pressure (PDF)

AUTHOR INFORMATION

Corresponding Authors

Lin Wang − *Center for High Pressure Science & Technology Advanced Research, Shanghai 201203, P. R. China; Center for High Pressure Science (CHiPS), State Key Laboratory of Metastable Materials Science and Technology, Yanshan University, Qinhuangdao, Hebei 066004, P. R. China;* orcid.org/0000-0003-2931-7629; Email: linwang@ysu.edu.cn

Jaeyong Kim − *Department of Physics and Institute for High Pressure, Hanyang University, Seoul 04763, Korea;* orcid.org/0000-0003-1787-3775; Email: kimjy@hanyang.ac.kr

Youngjong Kang − *Department of Chemistry, Institute of Nano Science and Technology, and Research Institute for Natural Sciences, Hanyang University, Seoul 04763, Korea;* orcid.org/0000-0001-5298-9189; Email: youngjkang@hanyang.ac.kr

Authors

Lan Anh Thi Nguyen − *Department of Physics and Institute for High Pressure, Hanyang University, Seoul 04763, Korea*

Duong Nguyen Minh − *Department of Chemistry, Hanyang University, Seoul 04763, Korea*

Dongzhou Zhang − *Partnership for Extreme Crystallography, University of Hawaii at Manoa, Honolulu, Hawaii 96822, United States*

Complete contact information is available at: https://pubs.acs.org/10.1021/acs.jpcc.0c06405

Notes

The authors declare no competing financial interest.

ACKNOWLEDGMENTS

This research was supported by Basic Science Research Program through the National Research Foundation of Korea (NRF) funded by the Ministry of Education, Science, and Technology (NRF-2016K1A4A3914691, 2018R1D1A1B07049811, 2019M1A7A1A03088471, 2018K1A3A1A32053991, 2012R1A6A1029029, and 2019K2A9A1A06071525). High-pressure XRD data were recorded at GeoSoilEnviroCARS (Sector 13), Partnership for Extreme Crystallography program (PX^2), Advanced Photon Source (APS), and Argonne National Laboratory. Partial XRD data were measured at the 5A beamline of the Pohang

Accelerator Laboratory (PAL), Korea. GeoSoilEnviroCARS is supported by the National Science Foundation-Earth Sciences (EAR-1634415) and Department of Energy-Geosciences (DE-FG02-94ER14466). PX^2 program is supported by COMPRES under NSF Cooperative Agreement EAR-1661511. Use of the Advanced Photon Source was supported by the US Department of Energy, Office of Science, Office of Basic Energy Sciences, under Contract No. DE-AC02-06CH11357.

REFERENCES

(1) Podzorov, V.; Pudalov, V.; Gershenson, M. Light-Induced Switching in Back-Gated Organic Transistors with Built-in Conduction Channel. *Appl. Phys. Lett.* **2004**, *85*, 6039−6041.
(2) Sirringhaus, H. Reliability of Organic Field-Effect Transistors. *Adv. Mater.* **2009**, *21*, 3859−3873.
(3) Kojima, A.; Teshima, K.; Shirai, Y.; Miyasaka, T. Organometal Halide Perovskites as Visible-Light Sensitizers for Photovoltaic Cells. *J. Am. Chem. Soc.* **2009**, *131*, 6050−6051.
(4) Lee, M. M.; Teuscher, J.; Miyasaka, T.; Murakami, T. N.; Snaith, H. J. Efficient Hybrid Solar Cells Based on Meso-Superstructured Organometal Halide Perovskites. *Science* **2012**, *338*, 643−647.
(5) Heo, J. H.; Im, S. H.; Noh, J. H.; Mandal, T. N.; Lim, C.-S.; Chang, J. A.; Lee, Y. H.; Kim, H.-j.; Sarkar, A.; Nazeeruddin, M. K.; et al. Efficient Inorganic−Organic Hybrid Heterojunction Solar Cells Containing Perovskite Compound and Polymeric Hole Conductors. *Nat. Photonics* **2013**, *7*, 486−491.
(6) Fang, Y.; Dong, Q.; Shao, Y.; Yuan, Y.; Huang, J. Highly Narrowband Perovskite Single-Crystal Photodetectors Enabled by Surface-Charge Recombination. *Nat. Photonics* **2015**, *9*, 679−686.
(7) Cho, H.; Jeong, S.-H.; Park, M.-H.; Kim, Y.-H.; Wolf, C.; Lee, C.-L.; Heo, J. H.; Sadhanala, A.; Myoung, N.; Yoo, S.; et al. Overcoming the Electroluminescence Efficiency Limitations of Perovskite Light-Emitting Diodes. *Science* **2015**, *350*, 1222−1225.
(8) Dong, Y.; Wang, Y.-K.; Yuan, F.; Johnston, A.; Liu, Y.; Ma, D.; Choi, M.-J.; Chen, B.; Chekini, M.; Baek, S.-W.; et al. Bipolar-Shell Resurfacing for Blue Leds Based on Strongly Confined Perovskite Quantum Dots. *Nat. Nanotechnol.* **2020**, *15*, 668−674.
(9) Wu, L.; Hu, H.; Xu, Y.; Jiang, S.; Chen, M.; Zhong, Q.; Yang, D.; Liu, Q.; Zhao, Y.; Sun, B.; et al. From Nonluminescent Cs_4PbX_6 (X= Cl, Br, I) Nanocrystals to Highly Luminescent $CsPBX_3$ Nanocrystals: Water-Triggered Transformation through a CsX-Stripping Mechanism. *Nano Lett.* **2017**, *17*, 5799−5804.
(10) Akkerman, Q. A.; Park, S.; Radicchi, E.; Nunzi, F.; Mosconi, E.; De Angelis, F.; Brescia, R.; Rastogi, P.; Prato, M.; Manna, L. Nearly Monodisperse Insulator Cs_4PbX_6 (X= Cl, Br, I) Nanocrystals, Their Mixed Halide Compositions, and Their Transformation into Cs PbX_3 Nanocrystals. *Nano Lett.* **2017**, *17*, 1924−1930.
(11) Palazon, F.; Urso, C.; De Trizio, L.; Akkerman, Q.; Marras, S.; Locardi, F.; Nelli, I.; Ferretti, M.; Prato, M.; Manna, L. Postsynthesis Transformation of Insulating Cs_4PbBr_6 Nanocrystals into Bright Perovskite $CsPbBr_3$ through Physical and Chemical Extraction of CsBr. *ACS Energy Lett.* **2017**, *2*, 2445−2448.
(12) Zheng, W.; Lin, R.; Ran, J.; Zhang, Z.; Ji, X.; Huang, F. Vacuum-Ultraviolet Photovoltaic Detector. *ACS Nano* **2018**, *12*, 425−431.
(13) Zheng, W.; Lin, R.; Zhu, Y.; Zhang, Z.; Ji, X.; Huang, F. Vacuum Ultraviolet Photodetection in Two-Dimensional Oxides. *ACS Appl. Mater. Interfaces* **2018**, *10*, 20696−20702.
(14) Saidaminov, M. I.; Almutlaq, J.; Sarmah, S.; Dursun, I.; Zhumekenov, A. A.; Begum, R.; Pan, J.; Cho, N.; Mohammed, O. F.; Bakr, O. M. Pure Cs_4PbBr_6: Highly Luminescent Zero-Dimensional Perovskite Solids. *ACS Energy Lett.* **2016**, *1*, 840−845.
(15) Zhang, Y.; Saidaminov, M. I.; Dursun, I.; Yang, H.; Murali, B.; Alarousu, E.; Yengel, E.; Alshankiti, B. A.; Bakr, O. M.; Mohammed, O. F. Zero-Dimensional Cs_4PbBr_6 Perovskite Nanocrystals. *J. Phys. Chem. Lett.* **2017**, *8*, 961−965.
(16) Cha, J.-H.; Han, J. H.; Yin, W.; Park, C.; Park, Y.; Ahn, T. K.; Cho, J. H.; Jung, D.-Y. Photoresponse of $CsPbBr_3$ and Cs_4PbBr_6 Perovskite Single Crystals. *J. Phys. Chem. Lett.* **2017**, *8*, 565−570.
(17) Chen, D.; Wan, Z.; Chen, X.; Yuan, Y.; Zhong, J. Large-Scale Room-Temperature Synthesis and Optical Properties of Perovskite-Related Cs_4PbBr_6 Fluorophores. *J. Mater. Chem. C* **2016**, *4*, 10646−10653.
(18) Seth, S.; Samanta, A. Fluorescent Phase-Pure Zero-Dimensional Perovskite-Related Cs_4PbBr_6 Microdisks: Synthesis and Single-Particle Imaging Study. *J. Phys. Chem. Lett.* **2017**, *8*, 4461−4467.
(19) Han, D.; Shi, H.; Ming, W.; Zhou, C.; Ma, B.; Saparov, B.; Ma, Y.-Z.; Chen, S.; Du, M.-H. Unraveling Luminescence Mechanisms in Zero-Dimensional Halide Perovskites. *J. Mater. Chem. C* **2018**, *6*, 6398−6405.
(20) Zhang, L.; Zeng, Q.; Wang, K. Pressure-Induced Structural and Optical Properties of Inorganic Halide Perovskite $CsPbBr_3$. *J. Phys. Chem. Lett.* **2017**, *8*, 3752−3758.
(21) Xiao, G.; Cao, Y.; Qi, G.; Wang, L.; Liu, C.; Ma, Z.; Yang, X.; Sui, Y.; Zheng, W.; Zou, B. Pressure Effects on Structure and Optical Properties in Cesium Lead Bromide Perovskite Nanocrystals. *J. Am. Chem. Soc.* **2017**, *139*, 10087−10094.
(22) De Bastiani, M.; Dursun, I.; Zhang, Y.; Alshankiti, B. A.; Miao, X.-H.; Yin, J.; Yengel, E.; Alarousu, E.; Turedi, B.; Almutlaq, J. M.; et al. Inside Perovskites: Quantum Luminescence from Bulk Cs_4PbBr_6 Single Crystals. *Chem. Mater.* **2017**, *29*, 7108−7113.
(23) Nikl, M.; Mihokova, E.; Nitsch, K.; Somma, F.; Giampaolo, C.; Pazzi, G.; Fabeni, P.; Zazubovich, S. Photoluminescence of Cs4pbbr6 Crystals and Thin Films. *Chem. Phys. Lett.* **1999**, *306*, 280−284.
(24) De Matteis, F.; Vitale, F.; Privitera, S.; Ciotta, E.; Pizzoferrato, R.; Generosi, A.; Paci, B.; Di Mario, L.; Pelli Cresi, J. S.; Martelli, F.; et al. Optical Characterization of Cesium Lead Bromide Perovskites. *Crystals* **2019**, *9*, 280.
(25) Saba, M.; Cadelano, M.; Marongiu, D.; Chen, F.; Sarritzu, V.; Sestu, N.; Figus, C.; Aresti, M.; Piras, R.; Lehmann, A. G.; et al. Correlated Electron−Hole Plasma in Organometal Perovskites. *Nat. Commun.* **2014**, *5*, 1−10.
(26) Wenger, B.; Nayak, P. K.; Wen, X.; Kesava, S. V.; Noel, N. K.; Snaith, H. J. Consolidation of the Optoelectronic Properties of $CH_3NH_3PbBr_3$ Perovskite Single Crystals. *Nat. Commun.* **2017**, *8*, 1−10.
(27) Xu, J.; Huang, W.; Li, P.; Onken, D. R.; Dun, C.; Guo, Y.; Ucer, K. B.; Lu, C.; Wang, H.; Geyer, S. M.; et al. Imbedded Nanocrystals of $CsPbBr_3$ in Cs_4PbBr_6: Kinetics, Enhanced Oscillator Strength, and Application in Light-Emitting Diodes. *Adv. Mater.* **2017**, *29*, 1703703.
(28) Quan, L. N.; Quintero-Bermudez, R.; Voznyy, O.; Walters, G.; Jain, A.; Fan, J. Z.; Zheng, X.; Yang, Z.; Sargent, E. H. Highly Emissive Green Perovskite Nanocrystals in a Solid State Crystalline Matrix. *Adv. Mater.* **2017**, *29*, 1605945.
(29) Chen, X.; Zhang, F.; Ge, Y.; Shi, L.; Huang, S.; Tang, J.; Lv, Z.; Zhang, L.; Zou, B.; Zhong, H. Centimeter-Sized Cs_4PbBr_6 Crystals with Embedded $CsPbBr_3$ Nanocrystals Showing Superior Photoluminescence: Nonstoichiometry Induced Transformation and Light-Emitting Applications. *Adv. Funct. Mater.* **2018**, *28*, 1706567.
(30) Nguyen, L. A. T.; Minh, D. N.; Yuan, Y.; Samanta, S.; Wang, L.; Zhang, D.; Hirao, N.; Kim, J.; Kang, Y. Pressure-Induced Fluorescence Enhancement of Fa A $PbBr^{2+}$ A Composite Perovskites. *Nanoscale* **2019**, *11*, 5868−5873.
(31) Ma, Z.; Liu, Z.; Lu, S.; Wang, L.; Feng, X.; Yang, D.; Wang, K.; Xiao, G.; Zhang, L.; Redfern, S. A. T.; et al. Pressure-Induced Emission of Cesium Lead Halide Perovskite Nanocrystals. *Nat. Commun.* **2018**, *9*, 4506.
(32) Shi, Y.; Ma, Z.; Zhao, D.; Chen, Y.; Cao, Y.; Wang, K.; Xiao, G.; Zou, B. Pressure-Induced Emission (PIE) of One-Dimensional Organic Tin Bromide Perovskites. *J. Am. Chem. Soc.* **2019**, *141*, 6504−6508.
(33) Fang, Y.; Zhang, L.; Wu, L.; Yan, J.; Lin, Y.; Wang, K.; Mao, W. L.; Zou, B. Pressure-Induced Emission (PIE) and Phase Transition of a Two-Dimensional Halide Double Perovskite $(BA)_4AgBiBr_8$ (BA= $CH_3(CH_2)_3NH^{3+}$). *Angew. Chem., Int. Ed.* **2019**, *58*, 15249−15253.

https://dx.doi.org/10.1021/acs.jpcc.0c06405
J. Phys. Chem. C 2020, 124, 22291−22297

(34) Calistru, D. M.; Mihut, L.; Lefrant, S.; Baltog, I. Identification of the Symmetry of Phonon Modes in $CsPbCl_3$ in Phase IV by Raman and Resonance-Raman Scattering. *J. Appl. Phys.* **1997**, *82*, 5391−5395.

https://dx.doi.org/10.1021/acs.jpcc.0c06405
J. Phys. Chem. C 2020, 124, 22291−22297